

Cite this: *Phys. Chem. Chem. Phys.*, 2011, **13**, 17295–17303

www.rsc.org/pccp

PAPER

Differential diffusion effects on buoyancy-driven instabilities of acid–base fronts: the case of a color indicator

S. Kuster,^a L. A. Riolfo,^{ab} A. Zalts,^c C. El Hasi,^c C. Almarcha,^b
P. M. J. Trevelyan,^b A. De Wit^{*b} and A. D’Onofrio^{*a}

Received 14th April 2011, Accepted 26th July 2011

DOI: 10.1039/c1cp21185d

Buoyancy-driven hydrodynamic instabilities of acid–base fronts are studied both experimentally and theoretically in the case where an aqueous solution of a strong acid is put above a denser aqueous solution of a color indicator in the gravity field. The neutralization reaction between the acid and the color indicator as well as their differential diffusion modifies the initially stable density profile in the system and can trigger convective motions both above and below the initial contact line. The type of patterns observed as well as their wavelength and the speed of the reaction front are shown to depend on the value of the initial concentrations of the acid and of the color indicator and on their ratio. A reaction-diffusion model based on charge balances and ion pair mobility explains how the instability scenarios change when the concentration of the reactants are varied.

1. Introduction

Studies of the influence of chemical reactions on convective mixing are currently receiving increasing attention, not only because of its industrial relevance¹ but also due to its crucial importance in CO₂ sequestration, *i.e.* in the storage of this greenhouse gas into geological formations. Indeed, buoyancy-driven motion occurs naturally when CO₂ dissolves into the brine of saline aquifers leading to denser CO₂ saturated zones sinking into the less dense brine.² Such a convective motion is favorable as it increases storage security. The potential influence of porous matrix dissolution or density changes by reactions is however difficult to assess *in situ*.

In this context, it is of interest to devise simple laboratory-scale experiments to study the relative role of reactions and transport processes in convective instabilities in order to understand the complex dynamics of sequestration and dispersion of reactive chemicals in porous media. Effectively, a series of experiments have recently analyzed convective mixing at the contact interface between two initially separated miscible solutions.^{2–4} Theoretical work also explains the various hydrodynamic instability scenarios that can be observed in such cases where a solution of a solute A is put on top of a miscible solution of another solute B.⁵

Those studies, however, do not consider the influence that chemical reactions can have on the density profile in the system.

In this respect, recent experiments also taking chemical reactions into account have been developed.^{6–9} The reactive solutions are contained in so-called Hele-Shaw cells, *i.e.* between two transparent glass or plastic plates ensuring a quasi-2D geometry and easy visualization of the dynamics. One solution containing an acid is put on top of another miscible denser solution containing another reactant. As the initial density stratification features a less dense solution on top of a denser one, convective instability can only come from double diffusive instabilities or changes in the density profile induced by reactions and diffusion. In the case where an aqueous solution of HCl is put on top of an equimolar solution of NaOH in the absence of any color indicator, convective patterns visualized by interferometry appear quite quickly after less than one minute.⁷ These convective motions develop in the form of plumes ascending above the initial contact line. They result from the fact that the acid diffuses faster downwards than the base diffuses upwards which creates a local minimum in density above the contact line where the richer acid solution overlies the less dense acid depleted zone. This differential diffusion effect triggers thus locally an unfavorable density stratification instability and is therefore called a diffusive layer convection mechanism.^{5,10} If a color indicator is added to the lower alkaline solution,^{6,8} different patterns are observed and in particular, a convective deformation of the reaction front traveling downwards in the basic solution is obtained. This has been shown to be due to the influence of the color indicator concentration on the density profile in the system.⁸ Buoyancy-driven convection

^a Grupo de Medios Porosos, Facultad de Ingeniería, Universidad de Buenos Aires, Paseo Colón 850, Buenos Aires, Argentina.
E-mail: adonofr@fi.uba.ar

^b Nonlinear Physical Chemistry Unit, Service de Chimie Physique et Biologie Théorique, Université Libre de Bruxelles (ULB), Campus Plaine, 1050 Brussels, Belgium. E-mail: adewit@ulb.ac.be

^c Instituto de Ciencias, Universidad Nacional General Sarmiento, J. M. Gutiérrez 1150, B1613GSX, Los Polvorines, Provincia de Buenos Aires, Argentina

around reactive fronts is therefore clearly affected by differential diffusion effects and by the presence of color indicators.

In this context, a clarification of the different possible types of dynamics is needed when the diffusion coefficients of the two initially separated reactants are very different and in particular when the reactant in the lower denser solution is almost immobile. It is indeed important to decipher the possible instability scenarios when CO_2 reacts with immobile reactants trapped for instance on the porous matrix of geological formations. In parallel, it is also important to understand in detail the active role that color indicators can play in reaction-diffusion-convection patterns studied at the laboratory scale. Indeed, these color indicators are often used in model experimental systems for visualization purposes where they are assumed to be passive scalars.²⁻⁴ However, recent results clearly show that they can affect the instabilities observed.⁸ Thus understanding their effect as a function of their relative concentration with the other chemicals is needed. This will enlighten the conditions under which they can be used or not for visualization purposes.

To address the above issues, we experimentally study convective instabilities of reaction fronts when a solution of a strong acid is placed on top of a solution of a color indicator in the gravity field. Here the color indicator is playing the role of a base and reacts with the acid in a fast neutralization reaction. Our study aims at clarifying the role of differential diffusion effects and of the color indicator in the dynamics and is therefore twofold. First, as the color indicator is a large and slow diffusing molecule while the acid is one of the fastest available species, we analyze the influence of strong differential diffusion effects on hydrodynamic instabilities of chemical fronts. Second, we highlight the crucial active role that a color indicator plays in spatio-temporal dynamics of reactive fronts, insisting on the fact that such indicators cannot usually be considered as passive scalars in any experimental studies of dynamics in solution in the gravity field.

Specifically, we conduct a parametric study of the instabilities induced by density changes of the reaction between hydrochloric acid and bromocresol green, a color indicator. We analyze the patterns observed, the temporal growth of the finger's length and the wavenumber of the pattern as a function of the initial concentration of the reactants and of the ratio of their initial concentrations. A reaction-diffusion model is used to construct density profiles in the system and understand the dynamics observed.

2. Experimental system

2.1. Reactants and chemical reaction

We focus on a simple neutralization reaction between an inorganic strong acid (hydrochloric acid, HCl) and a color indicator (bromocresol green), an organic basic salt with $\text{p}K_{\text{a}} = 5.3$. The reactants were chosen so that there was a neutralization reaction between a strong acid and a color indicator while maximizing the difference in diffusion coefficients.

HCl has one of the largest diffusion coefficients among the strong acids, while bromocresol green (BCG), with a large molecular mass ($\text{NaC}_{21}\text{H}_{13}\text{Br}_4\text{O}_5\text{S}$, $M_{\text{r}} = 863.03$), has a much

smaller diffusion coefficient than the acid, at least one order of magnitude smaller. Moreover the large difference between the molecular mass of HCl and BCG allows one to work with a considerably large difference in density, even if the reactant concentrations are similar. From the experimental point of view, BCG has a relatively high solubility in water, suitable to work with aqueous solutions, and a sharp color contrast between its acid (bright yellow-orange) and basic (dark blue) forms, enabling a good visualization of the reaction front position and pattern formation. The solutions were prepared using previously vacuumed distilled water, *i.e.* water which had been vacuumed for twenty-four hours to remove any air within it in order to avoid bubble formation inside the cell during the experiments. The densities were measured with a precision of $\pm 0.0001 \text{ g cm}^{-3}$ using an Anton Paar DMA 35N densitometer.

2.2. Set-up

The experiments were carried out in a quasi-two-dimensional system, a so-called Hele-Shaw cell widely used in the study of interfacial pattern formation.^{1-4,6-10} Here the experimental setup consists of two square Borofloat SCHOTT glass plates ($10 \text{ cm} \times 10 \text{ cm} \times 1.3 \text{ cm}$) separated by a U-shaped polymeric spacer of thickness $b = 1.0 \text{ mm}$. The spacer covers three sides of the cell, leaving the remaining side open (Fig. 1a). The dynamics takes place in the space between the plates. As the solutions used are reactive, in order to control the exact instant at which the chemical reaction starts and to ensure that the initial condition is a flat interface between the reactant solutions, we work with two Hele-Shaw (HS) cells filled separately and then put into contact. Both cells are fixed to an adjustable rotating frame, which allows the cells to be placed in either a horizontal or vertical position.

Each cell is filled through the "inlet" point (Fig. 1) with the corresponding reactant when the cells are in the horizontal position. Then, they are orientated towards the vertical position (parallel to the gravitational field), in a way that the cell containing the less dense reactant solution (the HCl solution in initial concentration A_0) is on top of the cell

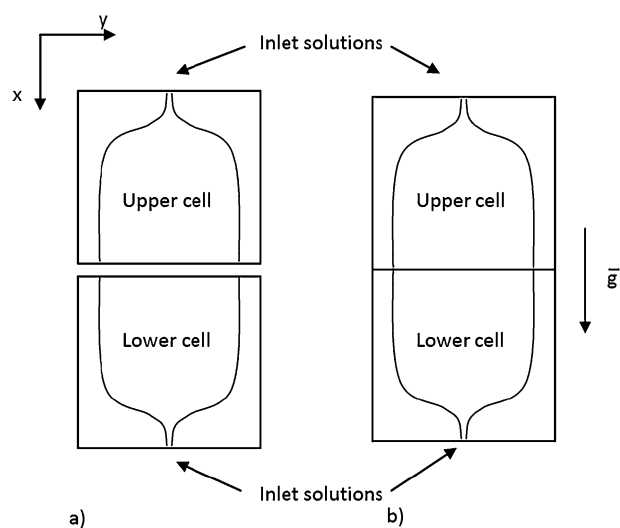


Fig. 1 Experimental set-up. (a) The cells are kept apart while the solutions are injected; (b) the cells are put into contact to start the reaction.

containing the denser reactant solution (the color indicator solution in initial concentration I_0). The acid solution in the upper cell does not flow out due to surface tension.⁶

In order to begin the experiment, the two HS cells are slowly brought into contact (Fig. 1b) and fixed together while the reaction starts. The HS cells are illuminated with transmitted diffuse white light from behind, and the experiments are recorded with a digital camera (3072×2304 pixels).

3. Results

As explained above, all of the experiments start with a less dense acid solution on top of a denser color indicator solution. From a hydrodynamic point of view, the initial condition in our experiments is thus a statically stable density stratification. However, after the cells are put into contact and the reaction starts, two different instability patterns can be observed in different regions depending on the initial reactant concentrations A_0 and I_0 and on the ratio

$$R = A_0/I_0$$

between them.

As an example of the instabilities that develop in the system, Fig. 2 shows selected images of the temporal evolution of the system with initial concentration $A_0 = 0.1$ M and

$I_0 = 0.02$ M ($R = 5$). Soon after cells have been put into contact, the acid–base reaction front, which is moving downwards in the lower cell, becomes unstable. The resulting instability creates a wave-like pattern between the yellow-orange (acid) and the dark blue (basic) zones (Fig. 2a). Later on, a different instability appears, with a larger wavelength, in the upper cell, where convective flows between plumes rising in the acid zone are observed (Fig. 2b and c).

In order to observe the influence of changes in the reactant concentrations and of the reactant concentration ratio R on the instabilities, various experiments summarized in Table 1 were performed.

The first row shows the changes when the concentration of the indicator solution is varied, holding A constant at 0.1 M. The second row on the contrary shows the changes when the concentration A was varied, holding $I = 0.01$ M. Let us note that, for these experiments, the optimal HCl concentrations range between 0.1 and 0.005 M because the solutions must be diluted enough to minimize the heat of dilution of the acid, yet concentrated enough to provide large enough density changes to observe convection on reasonable time scales. The concentrations used for the indicator were also limited by solubility (as it is impossible to obtain aqueous solutions more concentrated than 0.05 M), and by the limit of detection of the yellow form of the indicator.

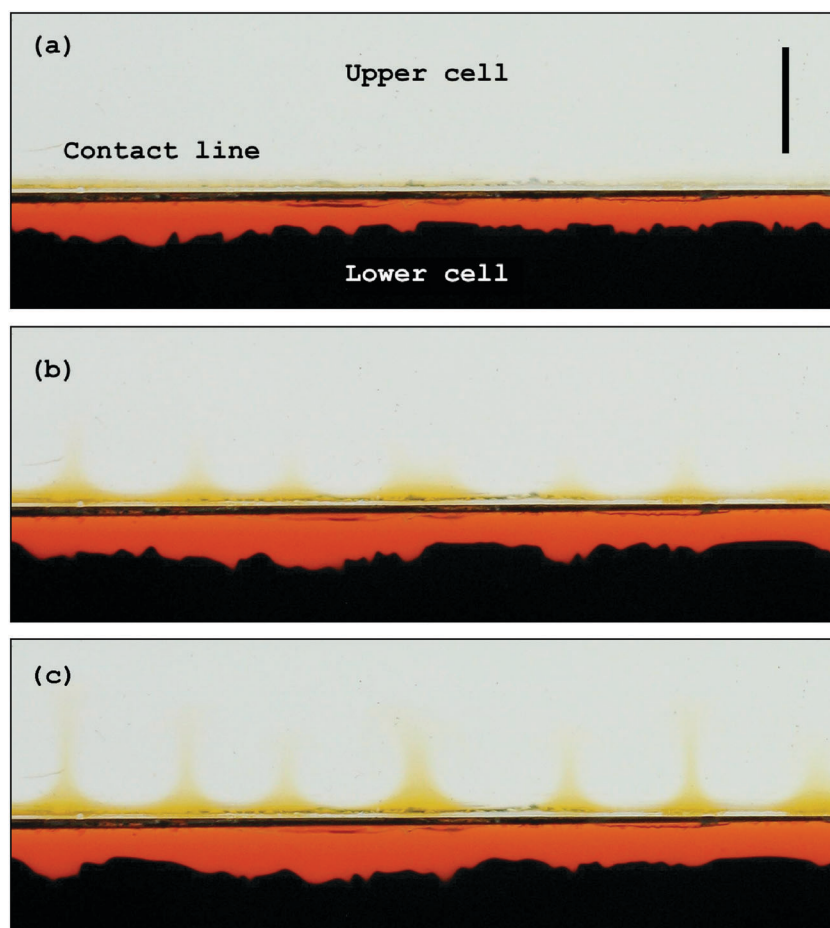







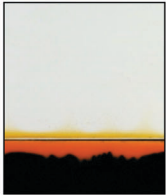



Fig. 2 Convective instabilities for $A_0 = 0.1$ M and $I_0 = 0.02$ M ($R = 5$) shown at (a) 155 s, (b) 355 s, (c) 455 s. The dark horizontal line in the middle is a shadow of the contact region between the upper and lower cells. The width of the field of view is 3.95 cm. The bar is 0.5 cm long.

Table 1 Convective patterns observed at $t = 1140$ s for various values of the initial concentrations of the acid A_0 and of the color indicator I_0 . In the 1st row, A_0 is constant for different I_0 concentrations while in the 2nd row, I_0 is constant for different A_0 concentrations. Each column corresponds to a fixed ratio R for various initial concentrations. Each field of view has a height of 3.69 cm. The bar is 0.7 cm

$R = 10$	$R = 5$	$R = 2$	$R = 0.5$	
$A_0 = 0.1$ M $I_0 = 0.01$ M 	$A_0 = 0.1$ M $I_0 = 0.02$ M 	$A_0 = 0.1$ M $I_0 = 0.05$ M 		Constant A_0
$A_0 = 0.1$ M $I_0 = 0.01$ M 	$A_0 = 0.05$ M $I_0 = 0.01$ M 	$A_0 = 0.02$ M $I_0 = 0.01$ M 	$A_0 = 0.005$ M $I_0 = 0.01$ M 	Constant I_0
	$A_0 = 0.035$ M $I_0 = 0.007$ M 	$A_0 = 0.04$ M $I_0 = 0.02$ M 		

As each panel of Table 1 is shown at the same time, we can conclude from these experiments that the system is more unstable when R is increased. Moreover, at fixed A_0 , the system is more unstable when I_0 is decreased while, at fixed I_0 , an increase in A_0 destabilizes the system. Let us show that these various trends can be understood on the basis of a reaction-diffusion model of the problem.

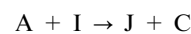
Let us note that the type of patterns can change depending on the color indicator used as shown by Tanoue *et al.*^{11,12} Their results are however difficult to be compared to those presented here because of the presence, in their recipes, of ethanol used to solubilize the indicator which is triggering Rayleigh–Taylor instabilities (upper layer denser than the lower one) in some cases.

4. Charge balances, ion-pair model and density profiles

To analyze the dynamics, we use a reaction-diffusion model based on charge balances and ion pair diffusion to explain how the instability scenarios change when the composition of the reactants is varied. This model not only explains the results

analyzed here, *i.e.* when a strong acid is on top of a color indicator, but has also proven to be useful in understanding dynamics in similar systems with an acid (HCl) aqueous solution on top of alkaline aqueous solutions of different reactants (either NaOH⁷ or another base⁹ alone or NaOH + BCG^{6,8}). The reactants, hydrochloric acid and bromocresol green, dissociate in the aqueous solution in the following way: in the upper HS cell, the acid dissociates as: $\text{H}_2\text{O} + \text{HCl} \rightarrow \text{Cl}^- + \text{H}_3\text{O}^+$ while in the bottom HS cell, the color indicator becomes: $\text{NaBCG} \rightarrow \text{Na}^+ + \text{BCG}^-$. The model assumes that (i) in maintaining the electroneutrality of the solution, each charged species diffuses in the solution as part of an ion pair rather than moving as a free ionic species; (ii) the diffusion coefficient of an ionic pair is constant and equal to that at infinite dilution; and (iii) the neutralization reaction is fast and irreversible.

To model this system, we denote I for NaBCG (the basic form of the color indicator), J for HBCG (the acid form of the color indicator), A for HCl (the acid) and C for the product NaCl (the salt). The neutralization reaction taking place is thus here



The corresponding reaction-diffusion equations for the concentrations A , I , J , C of the four relevant species A, I, J and C are then:

$$\frac{\partial A}{\partial t} = D_A \nabla^2 A - kAI$$

$$\frac{\partial I}{\partial t} = D_I \nabla^2 I - kAI$$

$$\frac{\partial J}{\partial t} = D_J \nabla^2 J + kAI$$

$$\frac{\partial C}{\partial t} = D_C \nabla^2 C + kAI$$

The diffusion coefficients for the acid HCl and the salt NaCl are,¹³ respectively, $D_A = 3.0 \times 10^{-9} \text{ m}^2 \text{ s}^{-1}$ and $D_C = 1.5 \times 10^{-9} \text{ m}^2 \text{ s}^{-1}$. For the color indicator species, according to its molecular weight,⁸ we take $D_I = D_J = 0.15 \times 10^{-9} \text{ m}^2 \text{ s}^{-1}$. Integrating the reaction-diffusion equations with an initial condition corresponding to two touching step functions with A in concentration A_0 and I in concentration I_0 with $J_0 = C_0 = 0$, we obtain evolving concentration profiles for each of the four species. From those profiles, assuming a linear dependence of the density with the species concentrations and the corresponding molar expansion coefficient [$\alpha_i = (1/\rho_0)(\partial\rho/\partial C_i)$] as the proportional constant, the density profile developed in the HS cell is reconstructed as:

$$\rho_{\text{tot}} = \rho_0 (1 + \alpha_A A + \alpha_I I + \alpha_C C + \alpha_J J)$$

The molar expansion coefficients, measured experimentally for each species, are:

$$\alpha_A = (0.018 \pm 0.001) \text{ M}^{-1}; \alpha_I = (0.385 \pm 0.001) \text{ M}^{-1};$$

$$\alpha_C = (0.038 \pm 0.001) \text{ M}^{-1}; \alpha_J = (0.370 \pm 0.001) \text{ M}^{-1}.$$

To obtain insight into density profiles, we plot the contribution $\rho_j = \alpha_j C_j$ of each species to density where C_j is the concentration of the related species j as a function of the self-similar variable $\eta = x/(4D_A t)^{1/2}$ where x is the vertical coordinate. Fig. 3 shows these contributions as well as the total dimensionless density profile $\rho^* = (\rho_{\text{tot}} - \rho_0)/\rho_0$ in the case when the initial concentrations A_0 of the acid and I_0 of the color indicator are both equal to 1 M. The difference in diffusion coefficients between the species plays a major role in the evolution of the system. The fast diffusion downwards of the acid creates, in the upper layer, a depletion zone where locally the acid solution in concentration A_0 overlies the zone depleted in the acid. This explains the instability observed in Fig. 2 in the upper layer.^{7,9} As the acid meets the basic form I of the color indicator, it reacts with it to give the acid form J which diffuses upwards in the upper layer. Because the acid diffuses much faster than the indicator in both its acid and basic forms, the reaction front is located further downwards around $\eta = -0.5$ which is largely inside the lower layer. The slow diffusion of the color indicator upwards does not compensate for the fast escape of the acid downwards which explains the depletion zone in the upper layer and the development of a maximum in density in the lower part of the system,

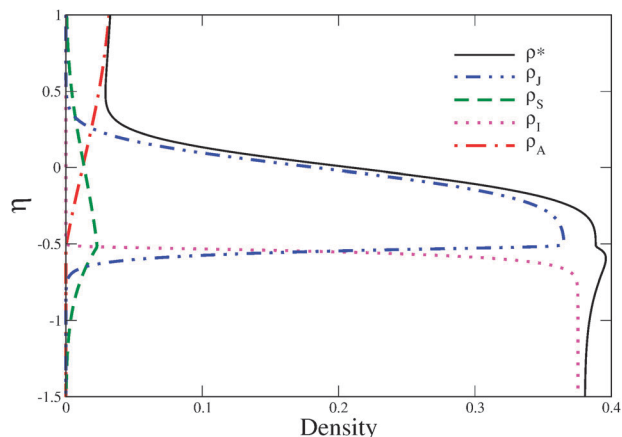


Fig. 3 Dimensionless total density profiles ρ^* as well as contributions $\rho_j = \alpha_j C_j$ to it of each species as a function of the self-similar variable $\eta = x/(4D_A t)^{1/2}$ for initial concentrations $A_0 = I_0 = 1 \text{ M}$.

reinforced by the accumulation of the product sodium chloride in the reaction zone. This leads to a locally unstable stratification responsible for the convective patterns observed in the lower layer in the reaction zone.^{6,8} This is different from the case of a base like NaOH for instance where the faster diffusion of this base and of the salt NaCl away from the lower layer prevents the build-up of a maximum in the lower layer.^{7,9} Note that even if the indicator diffuses much slower than the acid, its contribution to the density profile extends quite far in the upper layer because of its much larger solutal expansion coefficient.

Fig. 4 shows that an increase in the concentration of the acid above the base at fixed I_0 (increasing R) favors the development of two instabilities by increasing the relative amplitude of the depletion zone in the upper layer and that of the local maximum in the lower layer as confirmed in Table 1.

To understand the magnitude of the instability when A_0 is varied at fixed I_0 , let us introduce a dimensionless number DR that relates the local density jump in the extrema of the density profile to the global density jump between the acid and the color indicator. The larger the DR , the more important the unstable local stratification will be with regard to the overall system stability.

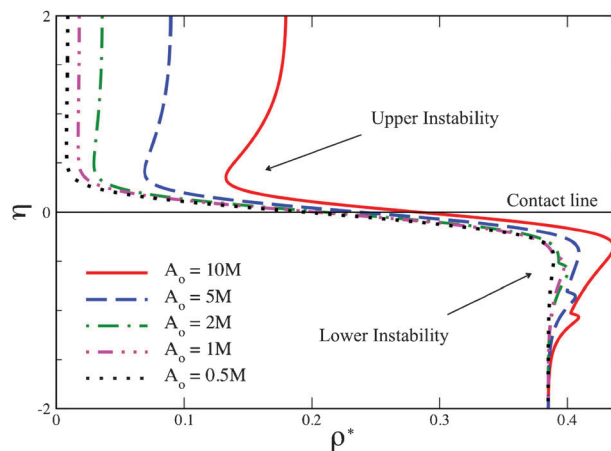


Fig. 4 Dimensionless density profiles for $I_0 = 1 \text{ M}$ and different values of A_0 .

Table 2 Contributions to density profiles for fixed I_0 and variable A_0

$I_0 = 1 \text{ M}$	$A_0 = 0.5 \text{ M}, R = 0.5$	$A_0 = 1 \text{ M}, R = 1$	$A_0 = 2 \text{ M}, R = 2$	$A_0 = 5 \text{ M}, R = 5$	$A_0 = 10 \text{ M}, R = 10$
ρ_{top}	1.0090	1.0180	1.0360	1.0900	1.1800
ρ_{bot}	1.3850	1.3850	1.3850	1.3850	1.3850
ρ_{min}	1.0080	1.0170	1.0290	1.0693	1.1327
ρ_{max}	1.3890	1.3980	1.4010	1.4087	1.4362
DR_{min}	2.660×10^{-3}	2.725×10^{-3}	2.006×10^{-2}	7.031×10^{-2}	2.306×10^{-1}
DR_{max}	1.064×10^{-2}	3.542×10^{-2}	4.585×10^{-2}	8.030×10^{-2}	2.496×10^{-1}

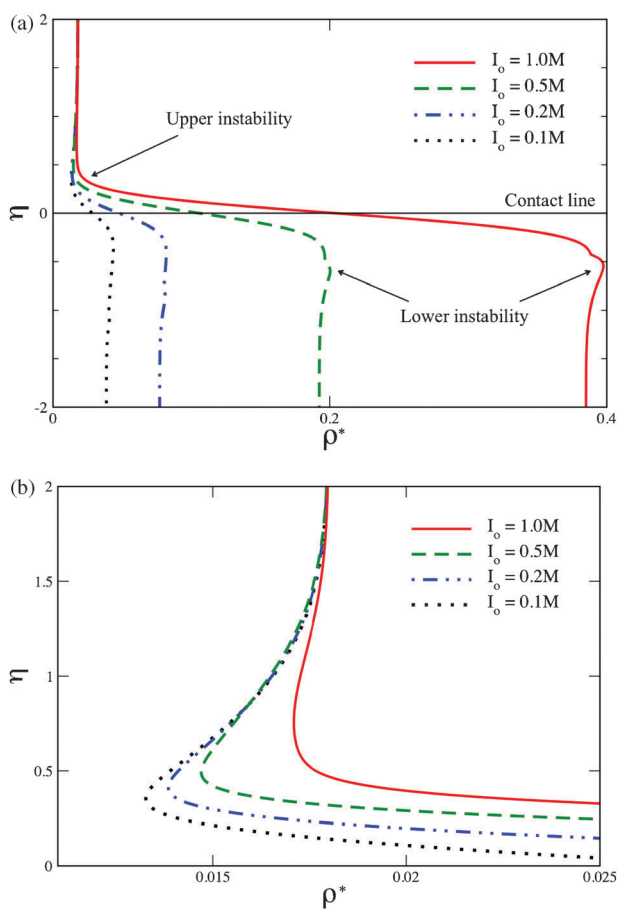
Specifically, we first define the global density jump $\Delta\rho = \rho_{\text{bot}} - \rho_{\text{top}}$ where ρ_{bot} is the initial density of the lower color indicator solution in concentration I_0 while ρ_{top} is the initial density of the upper acid solution in concentration A_0 . As we start from a less dense acid solution on top of a denser lower color indicator one, $\Delta\rho$ is always positive. We next detect on the numerical density profile the density ρ_{min} at the

minimum in the upper zone and the density ρ_{max} at the maximum in the lower zone.

We then define two different DR: $\text{DR}_{\text{min}} = (\rho_{\text{top}} - \rho_{\text{min}})/\Delta\rho$ and $\text{DR}_{\text{max}} = (\rho_{\text{max}} - \rho_{\text{bot}})/\Delta\rho$. Table 2 shows the corresponding ρ_{top} , ρ_{bot} , ρ_{min} , ρ_{max} and the respective DR_{min} and DR_{max} for each of the profiles shown in Fig. 4. From this table we can infer that, for a fixed I_0 , the larger the A_0 , the larger the DR_{min} and DR_{max} and hence the more unstable the system in both upper and lower layers. This is consistent with the experimental trends seen in Table 1.

Fig. 5 shows the density profiles when the initial concentration I_0 is varied for a fixed acid initial concentration A_0 . As in Fig. 4, two unstable regions can be observed. Table 3 shows the corresponding ρ_{top} , ρ_{bot} , ρ_{min} and ρ_{max} and the corresponding DR_{min} and DR_{max} for each of the profiles shown in Fig. 5. Thus, for a fixed A_0 , the larger the I_0 , the smaller the DR numbers and hence the less unstable the density configuration. This is again coherent with the observed experimental trend presented in Table 1.

It is also important to discuss heat effects. Neutralization reactions are typically exothermic reactions. However, it is found that the temperature contribution to the variation of density is negligible. Exothermicity indeed has a weak influence on convection as can be understood when comparing the solutal Rayleigh–Darcy numbers $R_A = \alpha_A A_0 g l_A K / (\nu D_A)$ for species A and the thermal number $R_T = \alpha_T \Delta T g l_T K / (\nu D_T)$ for temperature, where the characteristic lengths are $l_A = (D_A t)^{1/2}$ and $l_T = (D_T t)^{1/2}$ for acid and temperature profiles respectively. g is the intensity of gravity acceleration and K the permeability. The maximum value of temperature jump can be approximated to be $\Delta T = |\Delta H| I_0 / \rho_0 C_p$ in which, for $\Delta H = -57 \text{ kJ mol}^{-1}$ for a neutralization reaction, $\rho_0 = 1 \text{ kg l}^{-1}$, $C_p = 4.18 \text{ kJ kg}^{-1} \text{ K}^{-1}$ for water and the largest limiting concentration $I_0 = 0.05 \text{ M}$ used in Table 1 gives $\Delta T = 0.68 \text{ K}$. This is consistent with values measured for HCl–NaOH systems.^{11,12} Heat losses through the walls further decrease this maximum value which allows one to consider the physical properties of the problem (diffusion coefficient, viscosity for instance) as constant. In water for which $\alpha_T = -2.1 \times 10^{-4} \text{ K}^{-1}$ and $D_T = 1.35 \times 10^{-7} \text{ m}^2 \text{ s}^{-1}$, the ratio R_T/R_A

**Fig. 5** (a) Dimensionless density profiles for $A_0 = 1 \text{ M}$ and different values of I_0 . (b) Zoom on the density profiles in the upper region.**Table 3** Contributions to density profiles for fixed A_0 and variable I_0

$A_0 = 1 \text{ M}$	$I_0 = 0.1 \text{ M}, R = 10$	$I_0 = 0.2 \text{ M}, R = 5$	$I_0 = 0.5 \text{ M}, R = 2$	$I_0 = 1 \text{ M}, R = 1$
ρ_{top}	1.0180	1.0180	1.0180	1.0180
ρ_{bot}	1.0385	1.0770	1.1925	1.3850
ρ_{min}	1.0133	1.0139	1.0147	1.0170
ρ_{max}	1.0436	1.0818	1.2004	1.3980
DR_{min}	2.306×10^{-1}	7.032×10^{-2}	1.890×10^{-2}	2.725×10^{-3}
DR_{max}	2.496×10^{-1}	8.127×10^{-2}	4.499×10^{-2}	3.542×10^{-2}

expressing the relative weight of thermal *vs.* solutal effects in the density profile is estimated for $A_0 = 0.1$ M to be equal to 1.2×10^{-2} . Thus thermal effects can safely be neglected from the problem.

All the arguments extracted from the density profiles reconstructed on the basis of the reaction-diffusion model and the DR numbers are consistent with the experimental results in Table 1. More details about the agreement between the experiments and the theoretical explanations are further developed in the next section.

5. Discussion

5.1. Lower cell instabilities

As soon as the cells are brought into contact the acid–base neutralization reaction takes place, developing almost instantaneously hydrodynamic instabilities around the reaction front. The basic solution of color indicator I (dark blue bromocresol green) is neutralized by the acid A (HCl) to its acidic form J (yellow-orange color depending on the concentration).

The reaction front travels downwards, invading the basic solution, leaving behind an orange area upon transformation of I to J. Reaction-diffusion theory¹⁴ shows that the displacement speed of a reaction front $A + I \rightarrow J + C$ depends on $R = A_0/I_0$ and on the ratio $\delta = D_A/D_I$ of diffusion coefficients of the reactants A and I. If $R > 1$ and $\delta > 1$, then the flux of A towards the reaction zone is larger than that of I, and the front invades the region containing I. If no convective instability develops like for $R = 0.5$ for instance, the transport is only diffusive and lengths develop as $(D_A t)^{1/2}$ (Fig. 6). When R increases, convection sets in and transport is much faster as is also observed in horizontal cells for instance.^{15–17}

In the reaction front zone the density slightly increases due to the contribution of NaCl formation, the product of the chemical reaction and the fact that the color indicator barely escapes upwards. As a consequence, locally an unstable stratification develops and fingering-like patterns are observed

between the dark blue I and the yellow-orange J as soon as the front begins to propagate downwards (Fig. 2 and Table 1).

Fig. 6 shows the position of the reaction front as a function of time for different $R = A_0/I_0$ concentration ratios, according to Table 1. When experiments are performed with constant I_0 and variable A_0 , the reaction front travels faster downwards if convection is present when A_0 is increased (larger R). The same behavior is observed when the acid concentration is held constant by decreasing the base concentrations (larger R). Of course, this is consistent with the above reaction-diffusion theory¹⁴ but the magnitude of the increase is much too large to be explained in terms only of diffusion. In Fig. 6, four different reaction front speed tendencies are clearly observed, depending on R . The larger the R , the more unstable the system and the faster the front which is coherent with the fact that convection speeds up the front.

The temporal downward evolution of the reaction front depends thus on the concentration ratio R but over a wide concentration range, it is only weakly dependent on the absolute values of the concentrations themselves. So when $R = 2$ (corresponding to the various combinations $A_0 = 0.1$ M with $I_0 = 0.05$ M; $A_0 = 0.04$ M with $I_0 = 0.02$ M and $A_0 = 0.02$ M with $I_0 = 0.01$ M) the travelling front speed is almost the same for the three different combinations of initial reactant concentration. Similar is the situation observed for $R = 5$ (combining $A_0 = 0.1$ M with $I_0 = 0.02$ M; $A_0 = 0.05$ M with $I_0 = 0.01$ M and $A_0 = 0.035$ M with $I_0 = 0.007$ M) where the three cases have almost the same travelling front speed. For a given fixed R , the reaction front propagation speed is thus almost the same and only weakly dependent on the initial reactant concentration. This can be understood by noting that the DR values are roughly equal for a fixed R but different absolute (A_0, I_0) values in Tables 2 and 3. As an example, compare the DR values for $R = 10$ corresponding to $(A_0, I_0) = (10$ M, 1 M) in Table 2 and to $(A_0, I_0) = (1$ M, 0.1 M) in Table 3: they are exactly the same. A similar observation is made for $R = 2$ and 5 when comparing the two tables. Hence, we can understand that changing the absolute values of the initial concentration but maintaining R constant keeps

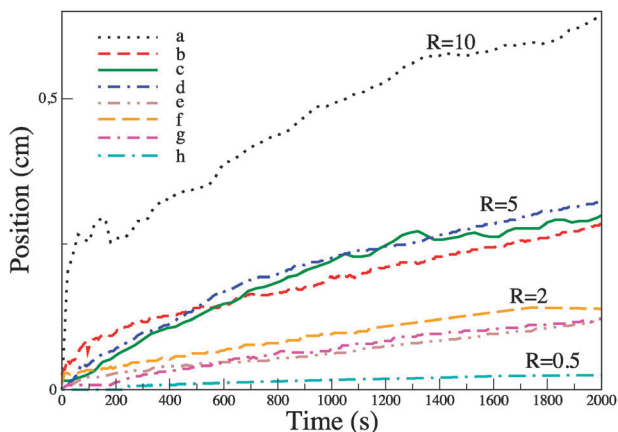


Fig. 6 Temporal evolution of the position of the reaction front for concentration pairs (A_0, I_0) equal to (a) (0.1 M, 0.01 M); (b) (0.1 M, 0.02 M); (c) (0.05 M, 0.01 M); (d) (0.035 M, 0.007 M); (e) (0.1 M, 0.05 M); (f) (0.04 M, 0.02 M); (g) (0.02 M, 0.01 M) and (h) (0.005 M, 0.01 M).

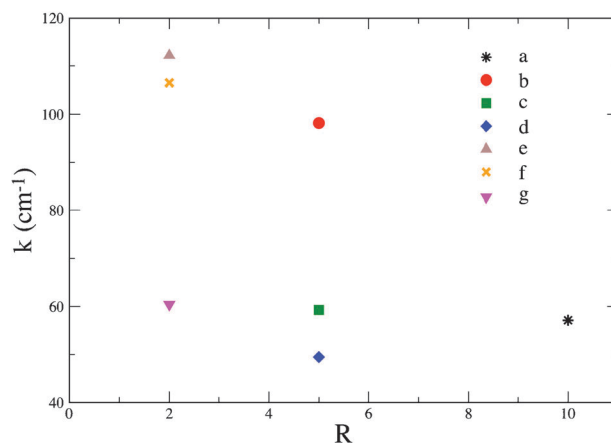


Fig. 7 Wavenumber k as a function of R , error on k values are 10^{-2} cm^{-1} for a couple of concentrations (A_0, I_0) equal to (a) (0.1 M, 0.01 M); (b) (0.1 M, 0.02 M); (c) (0.05 M, 0.01 M); (d) (0.035 M, 0.007 M); (e) (0.1 M, 0.05 M); (f) (0.04 M, 0.02 M) and (g) (0.02 M, 0.01 M).

DR *i.e.* the ratio between the jump in the extrema of the density profiles and the total density jump between the acid and the color indicator constant. This should therefore maintain the intensity of the convection rolls constant which explains that the temporal evolution of the front position is then similar. However, for increasing R , the larger the DR and hence the more intense the convection is, which explains why the fronts are traveling faster as seen in Fig. 6.

In parallel, the instabilities have also been characterized by their wavenumber at onset (when the instabilities began). This wavenumber is also related to the R parameter. Fig. 7 shows that increasing R at fixed A_0 , *i.e.* increasing DR, the averaged wavenumber k decreases. At a fixed R , the wavenumber increases when the absolute values of initial concentrations increase.

5.2. Upper cell instabilities

As the diffusion coefficient of J formed during the neutralization reaction is about ten times smaller than that of A , the faster invasion of A downwards produces a local density depletion on top of J , and convective cells appear above the initial contact line (see density profiles in Fig. 4 and 5). The instabilities produced by this depletion remain localized above the denser yellow J area. As there is no color indicator initially in the upper cell, such convective cells can be seen by interferometry⁷ or shadowgraphy⁸ for instance. Here, they are visualized by the yellow zones that are entrained upwards by convection.

The concentrations of A and J play an important role in both the formation and the visual detection of these instabilities. If solutions of A become too diluted, no instability can be formed anymore because there is no density minimum anymore. In this case, a flat yellow diffusion front moving upwards is observed.

When the initial concentration of A is kept constant in the upper cell and gives rise to a depletion zone, the system is less unstable when I_0 increases because DR decreases. This is coherent with the fact that, for a more concentrated J solution, the density of this solution is larger and can compensate, at least in part, the upper depletion. As a consequence, the time at which the first plumes are visible in the upper part increases (see Table 1 and Fig. 5b). For example, for a constant 0.1 M solution of A , the first plumes are visible after about 100 s for 0.01 M J , while for 0.02 M and 0.05 M J solutions, visualization occurred around 280 s and 430 s, respectively.

The instabilities in the upper cell are spatially and temporally independent from those produced in the lower cell. It can be seen that the wavenumber for the upper cell instabilities at later time is similar in all cases ($k \approx 1.77 \text{ cm}^{-1}$) but this corresponds obviously to later nonlinear dynamics stages. As there is no direct visualization of the wavenumber at onset in the upper zone, it is difficult to discuss its trend. Visualization by interferometry has in parallel given detailed analysis of this above pattern.⁷ We note however that in general the wavenumber in the upper layer is smaller than the one obtained in the lower cell instabilities ($k \approx 80 \text{ cm}^{-1}$). This can be related to the fact that systematically for all of the values of the parameters considered here, DR_{min} is smaller than DR_{max} . The instability is thus stronger in the lower region and hence the

corresponding most unstable wavenumber is larger *i.e.* the wavelength is smaller.

6. Conclusions

Chemical reactions can modify and influence hydrodynamic instabilities in systems where the reactants are initially put into contact in a statically stable density stratification. We have here analyzed in detail such an interplay between chemistry and fluid flows in a Hele-Shaw cell in the case where a strong acid solution is put on top of a denser solution of a color indicator acting here as a base in a neutralization reaction. Because of the large molecular weight of the color indicator and the fast diffusion of the acid, this choice of acid–base couple maximizes the differential diffusion effects between the reactants. Such a large difference in diffusion coefficients of the two reactants induces a depletion zone in the upper part above the initial contact line responsible for plume formation in the acidic zone and an accumulation of the product in the area of the reaction front where the color indicator barely diffuses. This creates a local maximum in density in the lower part of the reactor responsible for a spatial modulation of the reaction front traveling downwards. It is important to stress that such a maximum is not observed if other bases with a smaller molecular weight, which diffuse faster, are used.^{7,9} Destabilization of the reaction front in the lower layer is thus clearly related to the large difference in diffusion coefficients of the two reactants.

The kind of patterns observed and the onset time of the instabilities depend on the absolute and relative values of initial concentrations of the acid A_0 and the color indicator I_0 . The larger the ratio $R = A_0/I_0$, the more unstable the system both above and below the contact line. This is verified experimentally by both fixing A_0 and decreasing I_0 or fixing I_0 and increasing A_0 . Using a reaction-diffusion model and integrating the evolution equations for the concentrations of all chemical species involved, we have reconstructed the density profile in the cell for each experimentally studied case. This shows that increasing R increases DR values *i.e.* the relative intensity of the density jump in the local unstable stratification of the extrema with regard to the global density difference between the acid and the color indicator solutions.

Our results show that color indicators strongly affect the buoyancy-driven instabilities present in reactive solutions and should definitively be used with the strongest care to visualize convective dynamics. Moreover, we can also conclude that strong differential diffusion changes the type of the pattern obtained and that typically, if a species remains bounded on a porous matrix such as to have quasi zero effective diffusivity, the buoyancy-driven instabilities to be obtained are different to those in the non-reactive case^{2–5} or in reactive situations with smaller ratios of diffusion coefficients.^{6–9}

Acknowledgements

Our collaboration has benefitted from a MINCyT (Argentina)/FRS-FNRS (Belgium) bilateral cooperation programme which is gratefully acknowledged.

References

- 1 K. Eckert and A. Grahn, *Phys. Rev. Lett.*, 1999, **82**, 4436.
- 2 J. A. Neufeld, M. A. Hesse, A. Riaz, M. A. Hallworth, H. A. Tchelepi and H. E. Huppert, *Geophys. Res. Lett.*, 2010, **37**, L22404.
- 3 T. J. Kneafsey and K. Pruess, *Transp. Porous Media*, 2010, **82**, 123.
- 4 S. Backhaus, K. Turitsyn and R. E. Ecke, *Phys. Rev. Lett.*, 2011, **106**, 104501.
- 5 P. M. J. Trevelyan, C. Almarcha and A. De Wit, *J. Fluid Mech.*, 2011, **670**, 38.
- 6 A. Zalts, C. El Hasi, D. Rubio, A. Ureña and A. D'Onofrio, *Phys. Rev. E: Stat., Nonlinear, Soft Matter Phys.*, 2008, **77**, 015304(R).
- 7 C. Almarcha, P. M. J. Trevelyan, P. Grosfils and A. De Wit, *Phys. Rev. Lett.*, 2010, **104**, 044501.
- 8 C. Almarcha, P. M. J. Trevelyan, L. Riolfo, A. Zalts, C. El Hasi, A. D'Onofrio and A. De Wit, *J. Phys. Chem. Lett.*, 2010, **1**, 752.
- 9 C. Almarcha, Y. R'Honi, Y. De Decker, P. M. J. Trevelyan, K. Eckert and A. De Wit, *J. Phys. Chem. B*, 2011, **115**, 9739.
- 10 R. W. Griffiths, *J. Fluid Mech.*, 1981, **102**, 221.
- 11 K. Tanoue, M. Yoshitomi and T. Nishimura, *J. Chem. Eng. Jpn.*, 2009, **42**, 255.
- 12 K. Tanoue, H. Ikemoto, M. Yoshitomi and T. Nishimura, *Therm. Sci. Eng.*, 2009, **17**, 121.
- 13 *CRC Handbook of Chemistry and Physics*, ed. R. C. Weast and M. J. Astle, 59th edn, CRC Press, Boca Raton, FL, 1979.
- 14 L. Gálfi and Z. Rácz, *Phys. Rev. A*, 1988, **38**, 3151–3154.
- 15 Y. Shi and K. Eckert, *Chem. Eng. Sci.*, 2006, **61**, 5523.
- 16 L. Rongy, P. M. J. Trevelyan and A. De Wit, *Phys. Rev. Lett.*, 2008, **101**, 084503.
- 17 L. Rongy, P. M. J. Trevelyan and A. De Wit, *Chem. Eng. Sci.*, 2010, **65**, 2382.